Hindawi
Journal of Nanomaterials
Volume 2017, Article ID 2753934, 9 pages
https://doi.org/10.1155/2017/2753934

Research Article

Heat Dissipation of Resonant Absorption in Metal Nanoparticle-Polymer Films Described at Particle Separation Near Resonant Wavelength

Jeremy R. Dunklin[1] and D. Keith Roper[1,2]

[1]*Ralph E. Martin Department of Chemical Engineering, University of Arkansas, Fayetteville, AR 72701, USA*
[2]*Microelectronics-Photonics Graduate Program, University of Arkansas, Fayetteville, AR 72701, USA*

Correspondence should be addressed to D. Keith Roper; dkroper@uark.edu

Received 4 September 2016; Accepted 25 December 2016; Published 26 January 2017

Academic Editor: Ilaria Fratoddi

Polymer films containing plasmonic nanostructures are of increasing interest for development of responsive energy, sensing, and therapeutic systems. The present work evaluates heat dissipated from power absorbed by resonant gold (Au) nanoparticles (NP) with negligible Rayleigh scattering cross sections randomly dispersed in polydimethylsiloxane (PDMS) films. Finite element analysis (FEA) of heat transport was coordinated with characterization of resonant absorption by Mie theory and coupled dipole approximation (CDA). At AuNP particle separation greater than resonant wavelength, correspondence was observed between measured and CDA-predicted optical absorption and FEA-derived power dissipation. At AuNP particle separation less than resonant wavelength, measured extinction increased relative to predicted values, while FEA-derived power dissipation remained comparable to CDA-predicted power absorption before lagging observed extinguished power at higher AuNP content and resulting particle separation. Effects of isolated particles, for example, scattering, and particle-particle interactions, for example, multiple scattering, aggregation on observed optothermal activity were evaluated. These complementary approaches to distinguish contributions to resonant heat dissipation from isolated particle absorption and interparticle interactions support design and adaptive control of thermoplasmonic materials for a variety of implementations.

1. Introduction

Thermal damping of resonant nanoparticles (NPs) dispersed in optically transparent polymer could affect potential implementations in biomedical therapeutics [1, 2], solar cells [3–6], optical interconnects [7–9], sensing [10–12], and chemical separation [13]. Optical damping by subwavelength Mie scatterers [14] in the Rayleigh regime [15] whose scattering cross sections are negligible [16] is due to absorption [17]. Resonant power absorption of isolated nanoparticles [16] and colloid suspensions [18] in homogeneous dielectric environments is describable using Beer-Lambert linearization [19, 20] of Mie theory. Interactions between isolated subwavelength scatterers and their effects on absorption require more extensive characterization, such as dipole approximation [21, 22], finite difference time domain, or T-matrix. Additionally, interference to forward scattering, for example, reflection, refraction, or diffraction, due to an obstacle, [23] dielectric interface [24], applied field [25, 26], or other heterogeneity, may also impact optical extinction [27–29], thermal dynamics [30], and temperature dispersion [31–33]. Evaluation of heat dissipated from power absorbed in nanocomposites to distinguish contributions from isolated scatterers, interacting scatterers, and heterogeneity is important to advance understanding and guide design of thermally responsive nanocomposite materials.

Mie's solution to Maxwell's equations elegantly determines scattering and absorption of an electromagnetic plane wave by an isolated, homogenous sphere [34]. The solution, which depends on particle geometry, composition, surrounding dielectric medium, and angle of incidence, allows calculation of efficiencies and cross sections of scattering and absorption as well as intensity distributions. The coupled dipole approximation (CDA) to Maxwell's

equations incorporates Mie particle polarizability and also accounts for interparticle interactions [21, 22]. Multiplying the extinction cross section from homogeneous nanocomposite media containing spherical particles determined via Mie or CDA by the number of particles yields the overall optical response [35]. This is valid when absorbance is linearly proportional to concentration, as in Beer-Lambert law [17]. Beer-Lambert's law, $A = \sigma cl$, relates spectral absorbance, A, to AuNP concentration, c, and optical pathlength, l, using a material- and wavelength-specific absorbance coefficient, σ [17, 36]. Deviations from Mie and Beer-Lambert Law arise due to particle interactions, for example, multiple scattering, or strongly absorbing media [37, 38]. For nanoparticles in the Rayleigh regime with appreciable absorption cross section, damping of resonant absorption yields a strong photothermal response influenced by incident intensity, NP morphology [39, 40], and host media [41–43].

Heating by absorptive nanoparticles has been examined widely, but accounting for incident and dissipated energy by all mechanisms, that is, calibrating heat dissipated per unit absorption, is rare. Pulsed or continuous resonant irradiation of isolated NP or their assemblies is sufficient to reshape NP [44] and melt (evaporate) surrounding solids (liquids) [42, 45, 46]. The first comprehensive microscale calorimetric description of resonant absorption by NP in colloidal suspension analyzed dissipation via convection, conduction, and radiation [36, 47]. It has since been applied to quantitate resonant absorptive heating of NP deposited randomly on ceramic [41] and polymer [31] substrates and in multiphase [46], phase-change, and open [42] systems. Compact analytic expressions are useful to intuit dissipation and characterize thermal dynamics from geometric and thermodynamic nanocomposite features for effectively one-dimensional dissipation [30]. However, computational analysis remains necessary for systems with multidimensional absorption and dissipation. Correlating resonant absorption due to isolated particles by Mie theory and to particle interaction by CDA with heat dissipation by finite element analysis (FEA) for NPs dispersed randomly in multidimensional systems would increase understanding of these systems to support their integration into opto- and bioelectronic devices [48–51].

The present work used FEA to account for heat dissipation from ca. 1 mm thick PDMS films in which 16 nm AuNP with negligible Rayleigh scattering cross sections were randomly dispersed. Absorbed resonant power was characterized by Mie and CDA solutions. Power dissipation corresponding to measured and FEA-computed temperature profiles at thermal equilibrium was compared with estimates of extinguished power from Mie and CDA. Heat dissipated per unit absorption in AuNP-PDMS was consistent with reported optoplasmonic efficiencies for 15 to 18 nm AuNPs [52]. The compact description developed herein could be useful to guide intuition, design, and development of responsive plasmonic energy materials, sensors, MEMS, and therapeutics for heat-sensitive applications.

2. Materials and Methods

2.1. AuNP-PDMS Thin Film Fabrication. Briefly [29], polydimethylsiloxane (PDMS) films containing randomly dispersed AuNP were fabricated by mixing 1 mg/mL isopropanol suspension of 16 nm ± 2.4 nm diameter AuNP into uncured PDMS at increasing volumes to achieve AuNP concentrations ranging from 0.234 to 3.52×10^{12} NP/cm^3. Resulting mixtures were degassed, poured in polystyrene sample boxes, covered, and cured in an oven at 60°C for 24 h.

2.2. Optical Characterization. A light microscope (Eclipse LV100, Nikon Instruments, Melville, NY, USA) integrated with a spectrometer (Shamrock 303, Andor Technology, Belfast, UK) was used to measured AuNP-PDMS spectral response. Amplitudes at 532 nm, the excitation wavelength for subsequent thermal experiments, were determined as the difference between 532 nm extinction and extinction measured off-resonance (800 nm) for each sample. This accounted for contributions to extinction from the polymer matrix.

2.3. Mie Solution. Results from Mie solutions for isolated particles were obtained using a publicly available resource, http://nanocomposix.com/pages/tools. Simulations used a 16 nm AuNP in a refractive index corresponding to PDMS (1.42). For these conditions, resonant absorption cross sections for 16 nm AuNP are ~99% of total extinction. Mie cross sections are reported in nm^2 as a function of wavelength.

2.4. Coupled Dipole Approximation. The CDA [21, 53] treats the ith nanoparticle in an ensemble [54, 55] as a single dipole whose polarization is directly proportional to the local electric field [56]

$$\mathbf{P}_i = \alpha_i \mathbf{E}_{\text{tot}}(\mathbf{r}_i), \tag{1}$$

where α is a frequency-dependent polarizability and $\mathbf{E}_{\text{tot}}$ is the sum of incident irradiation ($\mathbf{E}_o$) and fields scattered from other particles in the lattice ($\mathbf{E}_{\text{lat}}$). Particle polarizability can be obtained analytically [55], computationally [56, 57], or by series approximations for higher order modes [58]. Effects of changing the angle of incident radiation can be evaluated [59]. The present work solved the CDA with a user-defined array by matrix inversion [51, 60]. Each dipole pair was calculated for a finite number of dipoles and superposed to determine the polarization vector, $\mathbf{P}_i$, at each dipole. Simulations in the present work were performed for 16 nm diameter spheres in a media refractive index for PDMS (1.42). A square 150 × 150 grid was used (90,601 dipoles) at a grating constant of double the Wigner-Seitz radius; $r_{\text{W-S}} = r_{\text{p}}(\rho_{\text{Au}}/x)^{1/3} = (3V/4\pi N)^{1/3}$, where r_{p} is the particle radius, ρ_{Au} is the density of gold (19.3 g/cm^3), x is gold mass per cubic centimeter of host media, V is the media volume, and N is the number of particles.

2.5. Thermal Characterization. Resonant laser irradiation of AuNP-PDMS was performed with a 532 nm laser (MXL-FN-532, CNI, Changchun, CN) with an intensity of ca. 25 mW. An infrared camera (ICI 7320, P-Series, Beaumont, TX, USA)

captured thermal images of the AuNP-PDMS at 5 Hz during a 10-second ambient capture, 2-minute-and-50-second heating (laser irradiation), and 3-minute cooling period. Tweezers were used to position AuNP-PDMS films such that the incident laser spot (~3 mm) was towards the top of the film, distal from the tweezer tip. Experimental apparatus was enclosed during data collection to minimize effects of forced convection. Each trial was performed in duplicate. Reported values were from a single representative trial.

2.6. Finite Element Analysis (FEA). Briefly [32], finite element analysis (FEA) used the Heat Transfer in Solids module in Version 5.2a of COMSOL Multiphysics (COMSOL, Stockholm, SE). Thermal equilibrium was simulated with an applied heat source that corresponded to laser irradiation for comparison with measured steady-state temperatures. Radiative, conductive, and convective cooling boundary conditions were used to estimate the rate at which heat was transferred to the surrounding environment (air). Thermal diffusivity controlled the developed temperature profile within the nanocomposite media. Measured two-dimensional AuNP-PDMS temperature profiles at the first instant of cooling were projected into the three-dimensional COMSOL geometry for comparison with steady-state simulated heating results.

The AuNP-PDMS films were assigned physical dimensions corresponding to measured height, length, and thickness. Each film had slightly different dimensions but was approximately $5 \times 5 \times 1$ mm. Values of density and specific heat capacity for each AuNP-PDMS film were estimated as weighted averages of respective values for Au and PDMS based on mass fraction of Au in the film. The thermal conductivity of AuNP-PDMS was assumed to be that of Au-free PDMS, as low mass fraction metallic dispersions in polymer have a negligible effect on bulk thermal conductivity [61]. Density, specific heat capacity, and thermal conductivity values for PDMS used were 970 kg/m^3, 1460 kJ/kg K, and 0.16 W/m K, respectively [62]. For Au, values used were 19320 kg/m^3, 128 J/kg K, and 317.9 W/mK [63], respectively.

Plasmonic heating from laser irradiation was represented by a Gaussian volumetric heat source centered at the measured laser spot center with a standard deviation of $r/2$, where r was the measured laser spot radius of ca. 1.5 mm. The full width at half maximum (FWHM) of this Gaussian distribution was 1.8 mm. Based on a raw incident laser intensity of 25 mW and this Gaussian function, the laser power incident on the sample, I, was estimated by centering the Gaussian function at the apparent laser spot center based on measured thermal results. This resulted in slightly suppressed powers ranging from 20 to 24 mW; that is, outer portions of the incident beam were off the sample. Spectral extinguished powers (E) were obtained from $E = I(1 - 10^{-A})$, where A was spectral extinction in absorbance units. Thermally dissipated power value was the fitting parameter in FEA used to match model-derived equilibrium temperature distributions with temperature distributions measured by the infrared camera at steady-state. Its value was adjusted until resulting FEA equilibrium maximum and minimum temperatures within the laser spot were within 0.1°C of measured steady-state values.

3. Results and Discussion

3.1. Optical Response Increased as Particle Separation Decreased below Resonant Wavelength. Measured optical responses of AuNP-PDMS films increased with NP concentration consistent with Mie and CDA results at low concentrations. However, when interparticle separation exceeded resonant wavelength, measured responses increased above calculated extinction. Figure 1(a) compares measured (solid), Mie (dotted), and CDA (dashed) spectra from PDMS films containing 16 nm AuNP at 1.17×10^{12} NP/cm^3 (0.005 mass-percent AuNP; blue) and 2.34×10^{12} NP/cm^3 (0.01 mass-percent AuNP; red). Spectral units are absorbance coefficient, calculated as optical extinction in absorbance units (AU) at 532 nm divided by sample thickness (mm), relative to off-resonance extinction at 800 nm. At 1.17×10^{12} NP/cm^3, the maximum extinction per mm for measured, Mie, and CDA values was 0.121, 0.140, and 0.120, respectively. At 2.34×10^{12} NP/cm^3, the maximum measured extinction per thickness was 0.313, thirty percent on average above Mie and CDA estimates of 0.252 and 0.23, respectively. Whether the 2.6-fold increase in optical response from a 2-fold rise in AuNP concentration translated to increased heat dissipation motivated further study.

This work defined extinction per NP to compare extinction in PDMS films containing 16 nm AuNP at concentrations ranging from 0.234 to 3.52×10^{12} NP/cm^3 [29]. Measured extinction per NP was calculated as AU/cnl, where AU was the extinction magnitude in absorbance units (AU), at 532 nm, c was the concentration in NP/cm^3, n was the spectrum-averaged refractive index of PDMS (1.42), and l was film thickness in cm. Extinction per NP was estimated from Mie theory as A/cnl using Beer-Lambert absorbance yielding extinction/NP=$\sigma(\log_{10}e)/n$, where σ was the Mie theory peak extinction cross section in cm^2, 2.78×10^{-12} cm^2, computed from an online tool (http://nanocomposix.com/pages/tools), and $\log_{10}e$ was a conversion factor between log-bases. Extinction per NP calculated from estimated Beer-Lambert absorption is thus independent of AuNP concentration. The output of CDA was extinction efficiency which was converted to an extinction cross section by multiplication by NP geometric cross section; that is, πr^2, where r was sphere radius of 8 nm. Extinction per NP was then estimated from CDA as $\sigma(\log_{10}e)/n$ using this cross section, 2.44×10^{-12} cm^2.

CDA was used to evaluate effects of interparticle interactions on extinction per NP. CDA results were computed using a square particle lattice with an interparticle separation distance double the Wigner-Seitz radius (upper-axis Figure 1(b)). The Wigner-Seitz radius, $r_{W\text{-}S}$, for a given particle concentration corresponds to the mean spherical volume of medium per particle. It is defined as $r_{W\text{-}S} = r_p(\rho_{Au}/x)^{1/3}$, where r_p is particle radius, ρ_{Au} is gold density (19.3 g/cm^3), and x is gold mass per cubic centimeter of PDMS. It was introduced in condensed matter physics to describe the

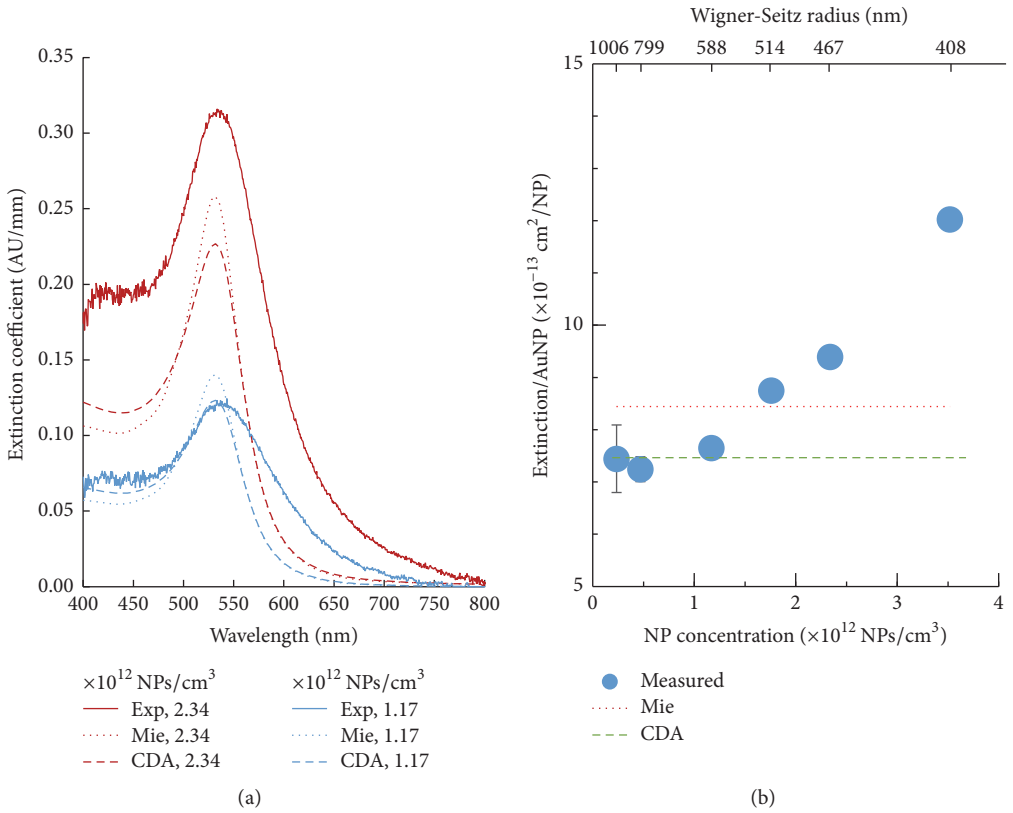

FIGURE 1: Optical response from AuNP-PDMS films increases when NP separation decreases below resonant wavelength. (a) Extinction coefficient (extinction/film thickness) based on experimental spectra (solid), Mie theory (dotted), and CDA (dashed) for AuNP-PDMS films containing 1.17 (blue) and 2.34 × 10^{12} NP/cm^3 (red). (b) Resonant extinction per AuNP in PDMS obtained from measured (blue circles) spectra, Mie theory (red dotted), and CDA (green dash). Positive and negative error bars correspond to adding and subtracting average signal noise from mean extinction value. This shows uncertainty due to noise ranged from 0.001 to 0.003 AU in measured extinction spectra. Data without visible bars had error within the size of the symbol.

density of a system [64] and estimates distance between NP in 3D dispersions [29, 32, 36].

Measured extinction per NP in AuNP-PDMS films was 9% lower on average than Mie and 2% higher on average than CDA estimates at AuNP concentrations for which the Wigner-Seitz radius, $r_{W\text{-}S}$, was greater than localized surface plasmon resonance wavelength, $\lambda_{LSPR} \sim 540$ nm; that is, $r_{W\text{-}S} \geq \lambda_{LSPR}$. For $r_{W\text{-}S} < \lambda_{LSPR}$, measured extinction per NP increased up to 1.4-fold relative to Mie and CDA estimates at the highest AuNP concentration. Figure 1(b) shows measured resonant extinction per NP for 16 nm AuNP with negligible scattering cross section randomly dispersed in PDMS films (blue circles). Corresponding results from the Mie (red dotted) and CDA (green dash) solutions are shown.

The top horizontal axis in Figure 1(b) shows that Wigner-Seitz radii decreased from 1006 nm to 408 nm as corresponding NP concentration on the bottom horizontal axis increased. Table 1 correlates AuNP concentration to Wigner-Seitz radius. At 1.76 × 10^{12} NP/cm^3, the first sample with Wigner-Seitz radii below the LSPR wavelength, extinction per NP measured in AuNP-PDMS films surpassed the corresponding Mie estimate (8.91 versus 8.45 × 10^{-13} cm^2/NP). Measured extinction per NP surpassed CDA estimates at 1.17 × 10^{12} NP/cm^3 (7.65 versus 7.41 × 10^{-13} cm^2/NP). As AuNP content increased, measured values diverged upward further from constant estimates, rising to a value of 12.0 × 10^{-13} cm^2/NP, 1.4- and 1.6-fold above values predicted using Mie and CDA at 3.52 × 10^{12} NP/cm^3. Depending on the mechanism producing it, an increase in optical extinction could benefit solar cells, as plasmon-induced electric fields and light scattering are reported to improve efficiency [6].

The observed increase in optical response for subwavelength particles randomly dispersed to interparticle distances less than the resonant wavelength could arise due to effects from isolated particles [15], particle-particle interactions [23], or optical interference, for example, dielectric heterogeneity [65]. The Mie results in Figure 1 correspond to resonant absorption from an isolated 16 nm Au nanosphere in the Rayleigh regime [15] whose scattering cross section is negligible [16]. Extinction per isolated AuNP in PDMS is constant since particle composition and dielectric environment remain unchanged. Optical effects of anomalous nonresonant scatterers in the AuNP-polymer matrix were removed by calculating resonant absorption by difference from off-resonant absorption at 800 nm. Control experiments were performed with AuNP-PDMS films containing 76 nm Au nanospheres with appreciable scattering cross section [29]. These films exhibited optical responses up to 1.3-fold greater

Table 1: Tabulated values of Wigner-Seitz radius, optically extinguished power from Mie and CDA, measured optically extinguished power, and fitted heat dissipated power based on FEA.

NP concentration ($\times 10^{12}$ NPs/cm^3)	Wigner-Seitz radius (nm)	Mie extinguished power (mW)	CDA extinguished power	Measured extinguished power (mW)	FEA fitted heat dissipated power (mW)
0.234	1006	1.40	1.23	1.299	0.88
0.469	799	3.26	2.86	2.82	2.38
1.17	588	6.57	5.77	6.32	4.87
1.76	518	11.7	10.3	12.12	9.49
2.34	467	9.90	8.69	10.7	9.08
3.52	408	14.9	13.1	17.8	11.5

than Mie estimates at $r_{W\text{-}S} > 4$ times the λ_{LSPR}, attributable to multiple scattering. Figure 1(b) indicates extinction per NP values consistent with Mie and CDA estimates at $r_{W\text{-}S} > \lambda_{LSPR}$. These results indicate scattering from isolated particles appears is unlikely from PDMS films containing 16 nm AuNP. Thus, isolated particle effects due to scattering from resonant or nonresonant scatterers appear unlikely to contribute significantly to increased optical response at or near resonance $r_{W\text{-}S} < \lambda_{LSPR}$.

Considering particle-particle interactions, the CDA results in Figure 1 correspond to collective extinction from one such 16 nm Au nanosphere interacting with others in a lattice. Extinction per NP decreases in CDA relative to Mie due to particle-particle interactions. Extinction per interacting AuNP in lattices at values of $r_{W\text{-}S}$ examined here remained constant since separation of particles with negligible scattering cross section remains sufficiently large, that is, in the far-field, such that negligible effect on the LSPR resonance accrues. Larger particles that resulted in appreciable scattering could accrue multiple scattering. Multiple scattering has been modeled by radiative transport and diffusive theory, typically for opaque samples that lack ballistic light transmission [66, 67]. However, negligible scattering cross sections for 16 nm AuNPs minimize effects of multiple scattering. On the other hand, near-field interactions at particle separation much less than $r_{W\text{-}S}$ values, that is, on the order of AuNP size (hot spots), have been reported to enhance resonance extinction [68, 69]. In this work, the 16 nm AuNPs studied were coated with ~10 nm polyvinylpyrrolidone (PVP) layer that diminished likelihood of such near-field interactions. This coating was observed to eliminated AuNP aggregation that was previously found after similar film fabrication using uncoated AuNP [31, 32]. In addition, LSPR wavelengths of AuNP-PDMS films blue-shifted as AuNP content increased from 542 to 532 nm rather than red-shifting as might be expected from near-field interaction. Moreover, optical responses of 16 nm AuNPs at up to 10^3 the concentrations evaluated here were within 12 and 17% of values predicted by CDA and Mie theory, respectively, in films sufficiently thin to preclude optical interference. Scanning electron microscope images of such films did not exhibit close particle interactions. Furthermore, random occurrence of such near-field interactions would not be expected to result in the observed linear divergence which was duplicated reproducibly at three particle concentrations. Therefore, particle-particle interactions appeared unlikely to contribute to increased optical response for $r_{W\text{-}S} < \lambda_{LSPR}$.

Considering optical interference, reproducible extinction per NP values consistent with Mie and CDA estimates at $r_{W\text{-}S} > \lambda_{LSPR}$ in Figure 1(b) indicate a prevailing optical interference arises only when interparticle distance decreases to values less than resonant wavelengths. The random distribution of the dispersed AuNP precludes optical interference from ordered scatterers, for example, lattice diffraction [51, 57, 58, 60, 68, 69]. Use of Maxwell Garnett effective medium theory [70, 71] to calculate change in effective dielectric constant due to increasing AuNP content yields extinction per NP estimates consistent with Mie and CDA. This absolves interference, for example, refraction, from dielectric heterogeneity. Geometric interference *alone*, for example, reflection at the PDMS-air interface [72], does not produce the increase at interparticle separation greater than $> \lambda_{LSPR}$. Remaining possibilities include diffraction in scattering systems, reported for coupled waveguides and photonic crystals [73], which could be measured using dynamic scattering, or time-averaged intensity of scattered light [74]. Control experiments with 76 nm AuNP with appreciable scattering cross section demonstrated that divergence of optical rays, for example, by multiple scattering or diffraction, convolved with internal reflection could increase observed extinction per AuNP relative to Mie-calculated values [29]. Thus, increased optical response for $r_{W\text{-}S} < \lambda_{LSPR}$ could be attributed to a geometric optical effect at the dielectric interface between polymer and air convolved with interference to incident radiation produced by adjacent resonant AuNP cross sections for $r_{W\text{-}S} < \lambda_{LSPR}$.

3.2. Heat Dissipation in AuNP-PDMS Films with Decreasing Interparticle Separation. Dissipation of power absorbed by AuNP dispersed in PDMS films was characterized by finite element analysis (FEA) using relations for heat conduction, natural convection, and radiation. Figure 2(a) compares measured (top) and simulated (bottom) temperature profiles for the 1.17×10^{12} NPs/cm^3 AuNP-PDMS film. A resonant absorbed power was introduced in order to calculate equilibrium temperature profiles that matched measured thermal profiles. Values for this power at consecutively higher AuNP contents increased from 1.2 to 11.1 mW as shown in Table 1, which summarizes optically extinguished powers and FEA-fitted heat dissipated powers. Measured, Mie, and

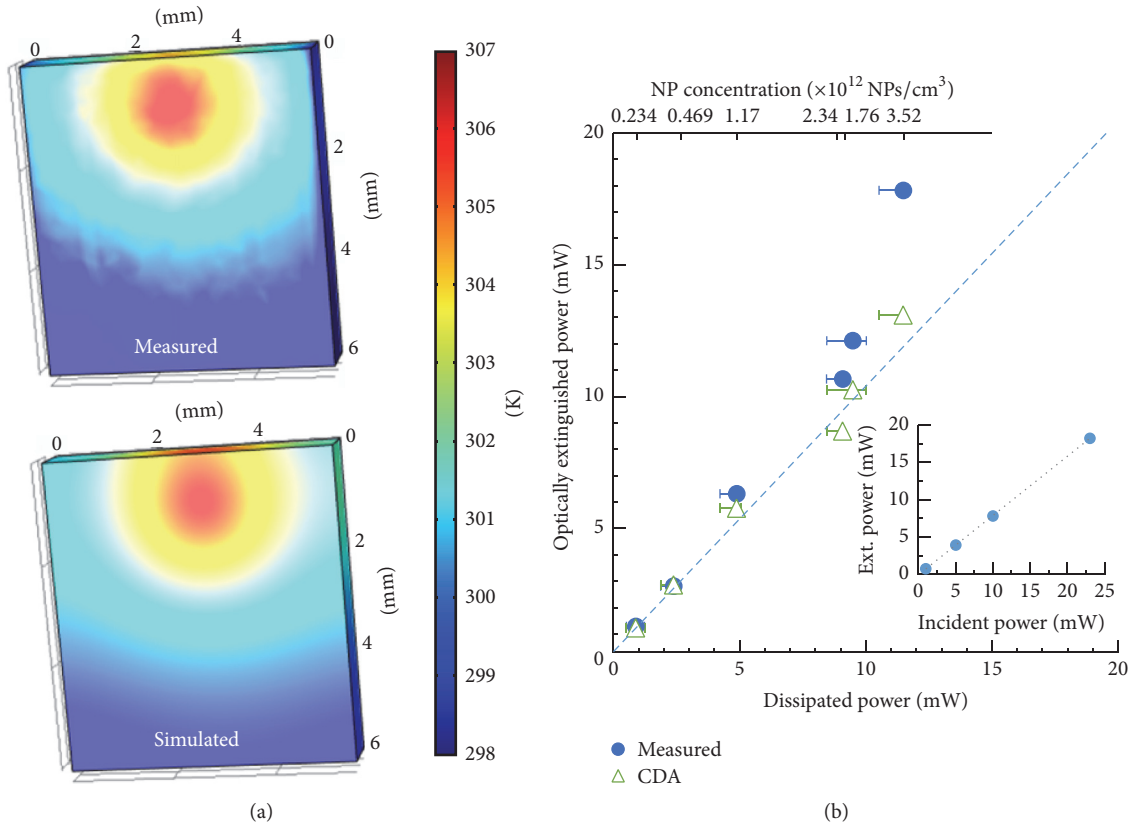

FIGURE 2: Measured extinction versus simulated absorption and heat dissipation. (a) Steady-state thermal profiles from FEA simulation (bottom), measurement (top) projected of the 1.17×10^{12} NPs/cm^3 AuNP-PDMS film. (b) Power dissipated thermally (x-axis) versus optically extinguished power (y-axis) taken from measured extinction and CDA estimates. Top-axis identifies NP concentration for each of six datasets. Inset shows linear increase in extinguished power with increased incident power for the 3.52×10^{12} NPs/cm^3 AuNP-PDMS film. Error bars in (b) result from upper- and lower-limit ambient temperature calculations.

CDA-predicted optically extinguished powers (E) were calculated as $E = I(1 - 10^{-A})$, where A was 532 nm spectral extinction in absorbance units, based on measured, Mie, and CDA theory, respectively, and I was incident power of 532 nm irradiation (19–24 mW) for each AuNP-PDMS film. Spectral extinction was estimated from Mie theory and CDA using Beer-Lambert absorbance [35] as reported in Section 3.1.

CDA-predicted optically extinguished power corresponded to FEA-fitted heat dissipated power derived from measured thermal response across the AuNP-PDMS films. Figure 2(b) plots FEA-derived thermal power dissipated (x-axis) versus optically extinguished power (y-axis) based on a priori CDA prediction (green hollow triangles) and measured optically extinguished power (filled blue circles). The blue dashed line indicates one-to-one correspondence. Overall agreement between CDA-predicted and FEA-derived powers at $r_{W\text{-}S} > \lambda_{LSPR}$, that is, AuNP $\leq 1.17 \times 10^{12}$ NP/cm^3, was consistent with ~98% agreement between CDA-derived and measured extinction per NP as shown in Figure 1(b). Incorporation of particle-particle interactions in CDA improved agreement with measured optical responses relative to Mie results, which reflected only isolated particle effects and are thus excluded from Figure 2(b).

For $r_{W\text{-}S} < \lambda_{LSPR}$, FEA-derived heat dissipated power lagged measured power values. The observed increase in extinction at these particle spacings appeared not to correspond to increased power dissipation. The optically extinguished power increased linearly with increasing incident power up to 25 mW, as shown in Figure 2(b) inset for the 3.52×10^{12} NPs/cm^3 AuNP-PDMS film. This suggests that neither aggregate thermal effects on particle and media dielectric values nor saturation measurably alters measured optical extinction relative to values obtained spectroscopically across the power and temperature ranges examined. Suppressed heat dissipation relative to optically extinguished power appeared attributable in part to edge effects. Temperature distributions of heated samples exceeded ambient values at film boundaries, particularly for off-center laser incidence. The heat transfer coefficients that were employed underpredicted heat transfer from the film's narrow vertical surface (~5 mm × ~1 mm) due to unaccounting for inward fluid flow induced near the edge. This effect has been reported to increase heat transfer rates by up to double for narrow, vertical surfaces [75]. As a result, modeled and measured temperature values diverged near film edges. Edge effects on geometric optics near film edges may have contributed to less power absorbed than that accounted for in measured extinction. Samples in which incident irradiation was at edges could have been affected by geometric optics, for example, reflection and refraction. FEA-derived heat dissipation

values were subject to user specification of absorbed power distributions in the FEA model which was important for characterizing sensitivity of incident beam distribution on resulting FEA-fitted heat source powers. The Gaussian power distribution used for all data shown enabled heat dissipated powers that reached an average temperature within the laser spot that matched measured results within 0.1°C. In contrast, uniformly distributing power over the 1.5 mm radius laser spot broadened the temperature profile with maximum (minimum) temperatures below (above) measured values. Decreasing power distribution radius to 0.5 mm resulted in maximum (minimum) temperatures above (below) measurements.

4. Conclusions

This work compared absorbed power derived from measured and predicted optical extinction with dissipated power obtained fitting measured temperature distributions to a finite element model in PDMS films containing 16 nm AuNPs with negligible scattering cross sections. Measured optical extinction corresponded to values predicted using CDA which accounted for particle-particle interactions at particle separation greater than resonance wavelength. Measured extinction exceeded CDA predictions at particle separation below resonance wavelength. Dissipated power estimated from measured temperature profiles corresponded to CDA-predicted optical extinction values at all particle separation studied. Spectroscopically measured extinction values corresponded to measured power extinguished up to 25 mW. But increases in spectroscopically measured extinction values relative to CDA-predicted extinction at particle separation less than resonance wavelength appeared to not result in corresponding increases in heat dissipation. Prediction of optical absorbance by Mie theory and coupled dipole approximation accounted for effects of isolated particle and particle-particle interactions, respectively, but not for interference with incidence radiation or dielectric heterogeneity, that is, geometric optical effects. Considered effects of near-field interactions and multiple scattering on measured optical responses did not appear significant for the particles studied. Coordinated examination of isolated particle, particle-particle, and dielectric heterogeneity effect on optothermal responses comparing experiment and theory is important to guide intuition, design, and development of responsive plasmonic energy materials for a variety of applications.

Disclosure

Any opinions, findings, and conclusions or recommendations expressed in this material are those of the authors and do not necessarily reflect the views of the National Science Foundation.

Competing Interests

The authors declare that there is no conflict of interests regarding the publication of this paper.

Acknowledgments

This work was supported in part by NSF CBET-1134222, NSF EEC-1260301, NSF Graduate Research Fellowship awarded to Jeremy R. Dunklin, the University of Arkansas Foundation, and the Walton Family Charitable Foundation. The authors graciously acknowledge Caitlyn Chambers for thermal data collection, Keith Berry, Jr. for conversion of temperature maps into three dimensions, and Gregory T. Forcherio for helpful discussions.

References

[1] T. Brann, D. Patel, R. Chauhan et al., "Gold nanoplates as cancer-targeted photothermal actuators for drug delivery and triggered release," *Journal of Nanomaterials*, vol. 2016, Article ID 2036029, 11 pages, 2016.

[2] O. Betzer, R. Ankri, M. Motiei, and R. Popovtzer, "Theranostic approach for cancer treatment: multifunctional gold nanorods for optical imaging and photothermal therapy," *Journal of Nanomaterials*, vol. 2015, Article ID 646713, 7 pages, 2015.

[3] F.-X. Xie, W. C. H. Choy, C. C. D. Wang, W. E. I. Sha, and D. D. S. Fung, "Improving the efficiency of polymer solar cells by incorporating gold nanoparticles into all polymer layers," *Applied Physics Letters*, vol. 99, no. 15, Article ID 153304, 2011.

[4] M. J. Mendes, S. Morawiec, T. Mateus et al., "Broadband light trapping in thin film solar cells with self-organized plasmonic nano-colloids," *Nanotechnology*, vol. 26, no. 13, Article ID 135202, 2015.

[5] H.-J. Kim, K. Y. Cho, S. S. Hwang, D. H. Choi, M. J. Ko, and K.-Y. Baek, "Controlled synthesis of multi-armed P3HT star polymers with gold nanoparticle core," *RSC Advances*, vol. 6, no. 54, pp. 49206–49213, 2016.

[6] M. Costa de Oliveira, A. L. Silveira Fraga, A. Thesing, R. Lopes de Andrade, J. Ferreira Leite Santos, and M. J. Leite Santos, "Interface dependent plasmon induced enhancement in dye-sensitized solar cells using gold nanoparticles," *Journal of Nanomaterials*, vol. 2015, Article ID 719260, 9 pages, 2015.

[7] Y.-Y. Noh, N. Zhao, M. Caironi, and H. Sirringhaus, "Downscaling of self-aligned, all-printed polymer thin-film transistors," *Nature Nanotechnology*, vol. 2, no. 12, pp. 784–789, 2007.

[8] Y.-C. Hung, T.-Y. Lin, W.-T. Hsu, Y.-W. Chiu, Y.-S. Wang, and L. Fruk, "Functional DNA biopolymers and nanocomposite for optoelectronic applications," *Optical Materials*, vol. 34, no. 7, pp. 1208–1213, 2012.

[9] C. O. Blattmann, G. A. Sotiriou, and S. E. Pratsinis, "Rapid synthesis of flexible conductive polymer nanocomposite films," *Nanotechnology*, vol. 26, no. 12, Article ID 125601, 2015.

[10] H. SadAbadi, S. Badilescu, M. Packirisamy, and R. Wüthrich, "Integration of gold nanoparticles in PDMS microfluidics for lab-on-a-chip plasmonic biosensing of growth hormones," *Biosensors and Bioelectronics*, vol. 44, no. 1, pp. 77–84, 2013.

[11] I. Venditti, I. Fratoddi, M. V. Russo, and A. Bearzotti, "A nanostructured composite based on polyaniline and gold nanoparticles: synthesis and gas sensing properties," *Nanotechnology*, vol. 24, no. 15, Article ID 155503, 2013.

[12] J. Lv, E. S. P. Leong, X. Jiang et al., "Plasmon-enhanced sensing: current status and prospects," *Journal of Nanomaterials*, vol. 2015, Article ID 474730, 10 pages, 2015.

[13] J. R. Dunklin, G. T. Forcherio, K. R. Berry, and D. K. Roper, "Asymmetric reduction of gold nanoparticles into thermoplasmonic polydimethylsiloxane thin films," *ACS Applied Materials and Interfaces*, vol. 5, no. 17, pp. 8457–8466, 2013.

[14] G. Mie, "Beiträge zur Optik trüber Medien, speziell kolloidaler Metallösungen," *Annalen der Physik*, vol. 330, no. 3, pp. 377–445, 1908.

[15] C. F. Bohren and D. R. Huffman, *Absorption and Scattering of Light By Small Particles*, John Wiley & Sons, New York, NY, USA, 1998.

[16] S. Berciaud, L. Cognet, P. Tamarat, and B. Lounis, "Observation of intrinsic size effects in the optical response of individual gold nanoparticles," *Nano Letters*, vol. 5, no. 3, pp. 515–518, 2005.

[17] K. C. Grabar, R. G. Freeman, M. B. Hommer, and M. J. Natan, "Preparation and characterization of Au colloid monolayers," *Analytical Chemistry*, vol. 67, no. 4, pp. 735–743, 1995.

[18] S. Kubo, A. Diaz, Y. Tang, T. S. Mayer, I. C. Khoo, and T. E. Mallouk, "Tunability of the refractive index of gold nanoparticle dispersions," *Nano Letters*, vol. 7, no. 11, pp. 3418–3423, 2007.

[19] A. Slistan-Grijalva, R. Herrera-Urbina, J. F. Rivas-Silva, M. Ávalos-Borja, F. F. Castillón-Barraza, and A. Posada-Amarillas, "Classical theoretical characterization of the surface plasmon absorption band for silver spherical nanoparticles suspended in water and ethylene glycol," *Physica E: Low-Dimensional Systems and Nanostructures*, vol. 27, no. 1-2, pp. 104–112, 2005.

[20] G. A. Rance, D. H. Marsh, and A. N. Khlobystov, "Extinction coefficient analysis of small alkanethiolate-stabilised gold nanoparticles," *Chemical Physics Letters*, vol. 460, no. 1–3, pp. 230–236, 2008.

[21] E. M. Purcell and C. R. Pennypacker, "Scattering and absorption of light by nonspherical dielectric grains," *The Astrophysical Journal*, vol. 186, pp. 705–714, 1973.

[22] B. T. Draine and P. J. Flatau, "Discrete-dipole approximation for scattering calculations," *Journal of the Optical Society of America A*, vol. 11, no. 4, pp. 1491–1499, 1994.

[23] E. Hecht, *Optics*, Addison-Wesley, Incorporated, Boston, Mass, USA, 2002.

[24] A. W. Powell, N. Hjerrild, A. A. R. Watt, H. E. Assender, and J. M. Smith, "Directional plasmonic scattering from metal nanoparticles in thin-film environments," *Applied Physics Letters*, vol. 104, no. 8, Article ID 81110, 2014.

[25] Q. Zhao, X. P. Zhao, C. Z. Qu, and L. Q. Xiang, "Diffraction pattern and optical activity of complex fluids under external electric field," *Applied Physics Letters*, vol. 84, no. 11, pp. 1985–1987, 2004.

[26] J. Lobera and J. M. Coupland, "Optical diffraction tomography in fluid velocimetry: the use of a priori information," *Measurement Science and Technology*, vol. 19, no. 7, Article ID 074013, 2008.

[27] G. T. Forcherio and D. K. Roper, "Optical attenuation of plasmonic nanocomposites within photonic devices," *Applied Optics*, vol. 52, no. 25, pp. 6417–6427, 2013.

[28] J. R. Dunklin, G. T. Forcherio, and D. Keith Roper, "Geometric optics of gold nanoparticlepolydimethylsiloxane thin film systems," *Optical Materials Express*, vol. 4, no. 2, pp. 375–383, 2014.

[29] J. R. Dunklin, G. T. Forcherio, and D. Keith Roper, "Gold nanoparticle-polydimethylsiloxane films reflect light internally by optical diffraction and Mie scattering," *Materials Research Express*, vol. 2, no. 8, Article ID 085005, 2015.

[30] K. R. Berry, J. R. Dunklin, P. A. Blake, and D. K. Roper, "Thermal dynamics of plasmonic nanoparticle composites," *Journal of Physical Chemistry C*, vol. 119, no. 19, pp. 10550–10557, 2015.

[31] K. R. Berry Jr., A. G. Russell, P. A. Blake, and D. K. Roper, "Gold nanoparticles reduced in situ and dispersed in polymer thin films: optical and thermal properties," *Nanotechnology*, vol. 23, no. 37, Article ID 375703, 2012.

[32] J. R. Dunklin, G. T. Forcherio, K. R. Berry, and D. K. Roper, "Gold nanoparticle-polydimethylsiloxane thin films enhance thermoplasmonic dissipation by internal reflection," *Journal of Physical Chemistry C*, vol. 118, no. 14, pp. 7523–7531, 2014.

[33] J. R. Dunklin, G. T. Forcherio, K. R. Berry, and D. K. Roper, "Plasmon optics and thermal dissipation in nanocomposite thin films," *MRS Proceedings*, vol. 1788, no. 37, pp. 23–28, 2015.

[34] G. Mie, "Contributions to the optics of turbid media, particularly of colloidal metal solutions," *Annals of Physics*, vol. 25, no. 3, pp. 377–445, 1908.

[35] S. S. Martinos, "Comment on 'Experimental test of the Mie theory for microlithographically produced silver spheres'," *Physical Review B*, vol. 40, no. 12, p. 8558, 1989.

[36] D. K. Roper, W. Ahn, and M. Hoepfner, "Microscale heat transfer transduced by surface plasmon resonant gold nanoparticles," *Journal of Physical Chemistry C*, vol. 111, no. 9, pp. 3636–3641, 2007.

[37] A. N. Lebedev, M. Gartz, U. Kreibig, and O. Stenzel, "Optical extinction by spherical particles in an absorbing medium: application to composite absorbing films," *European Physical Journal D*, vol. 6, no. 3, pp. 365–373, 1999.

[38] W. C. Mundy, J. A. Roux, and A. M. Smith, "Mie scattering by spheres in an absorbing medium," *Journal of the Optical Society of America*, vol. 64, no. 12, pp. 1593–1597, 1974.

[39] M. Lisunova, J. R. Dunklin, S. V. Jenkins, J. Chen, and D. K. Roper, "The unusual visible photothermal response of free standing multilayered films based on plasmonic bimetallic nanocages," *RSC Advances*, vol. 5, no. 20, pp. 15719–15727, 2015.

[40] X. Wang, P. Wang, J. Wang et al., "Ultrasensitive and broadband MoS_2 photodetector driven by ferroelectrics," *Advanced Materials*, vol. 27, no. 42, pp. 6575–6581, 2015.

[41] W. Ann and D. K. Roper, "Transformed gold Island film improves light-to-heat transduction of nanoparticles on silica capillaries," *The Journal of Physical Chemistry C*, vol. 112, no. 32, pp. 12214–12218, 2008.

[42] A. G. Russell, M. D. McKnight, J. A. Hestekin, and D. K. Roper, "Thermodynamics of optoplasmonic heating in fluid-filled gold-nanoparticle-plated capillaries," *Langmuir*, vol. 27, no. 12, pp. 7799–7805, 2011.

[43] S. C. Dixon, W. J. Peveler, N. Noor, J. C. Bear, and I. P. Parkin, "Superhydrophobic Au/polymer nanocomposite films via AACVD/swell encapsulation tandem synthesis procedure," *RSC Advances*, vol. 6, no. 37, pp. 31146–31152, 2016.

[44] S. Link, Z. L. Wang, and M. A. El-Sayed, "How does a gold nanorod melt?" *Journal of Physical Chemistry B*, vol. 104, no. 33, pp. 7867–7870, 2000.

[45] H. H. Richardson, Z. N. Hickman, A. O. Govorov, A. C. Thomas, W. Zhang, and M. E. Kordesch, "Thermooptical properties of gold nanoparticles embedded in ice: characterization of heat generation and melting," *Nano Letters*, vol. 6, no. 4, pp. 783–788, 2006.

[46] D. K. Roper, A. G. Russell, M. D. McKnight, A. C. Sharp, J. A. Hestekin, and D. K. Roper, "Gold nanoparticles allow optoplasmonic evaporation from open silica cells with a logarithmic approach to steady-state thermal profiles," *Journal of Physical Chemistry C*, vol. 114, no. 22, pp. 10132–10139, 2010.

[47] M. P. Hoepfner and D. K. Roper, "Describing temperature increases in plasmon-resonant nanoparticle systems," *Journal of Thermal Analysis and Calorimetry*, vol. 98, no. 1, pp. 197–202, 2009.

[48] D. K. Roper, "Enhancing lateral mass transport to improve the dynamic range of adsorption rates measured by surface plasmon resonance," *Chemical Engineering Science*, vol. 61, no. 8, pp. 2557–2564, 2006.

[49] D. K. Roper, "Determining surface plasmon resonance response factors for deposition onto three-dimensional surfaces," *Chemical Engineering Science*, vol. 62, no. 7, pp. 1988–1996, 2007.

[50] D. K. Roper and S. Nakra, "Adenovirus type 5 intrinsic adsorption rates measured by surface plasmon resonance," *Analytical Biochemistry*, vol. 348, no. 1, pp. 75–83, 2006.

[51] D. K. Roper, W. Ahn, B. Taylor, and A. G. Dall'Asen, "Enhanced spectral sensing by electromagnetic coupling with localized surface plasmons on subwavelength structures," *IEEE Sensors Journal*, vol. 10, no. 3, pp. 531–540, 2010.

[52] K. Jiang, D. A. Smith, and A. Pinchuk, "Size-dependent photothermal conversion efficiencies of plasmonically heated gold nanoparticles," *Journal of Physical Chemistry C*, vol. 117, no. 51, pp. 27073–27080, 2013.

[53] B. T. Draine and P. J. Flatau, "Discrete-dipole approximation for periodic targets: theory and tests," *Journal of the Optical Society of America A: Optics and Image Science, and Vision*, vol. 25, no. 11, pp. 2693–2703, 2008.

[54] P. J. Flatau and B. T. Draine, "Fast near field calculations in the discrete dipole approximation for regular rectilinear grids," *Optics Express*, vol. 20, no. 2, pp. 1247–1252, 2012.

[55] D. Dejarnette, J. Norman, and D. K. Roper, "Spectral patterns underlying polarization-enhanced diffractive interference are distinguishable by complex trigonometry," *Applied Physics Letters*, vol. 101, no. 18, Article ID 183104, 2012.

[56] D. Dejarnette, P. Blake, G. T. Forcherio, and D. Keith Roper, "Far-field Fano resonance in nanoring lattices modeled from extracted, point dipole polarizability," *Journal of Applied Physics*, vol. 115, no. 2, Article ID 024306, 2014.

[57] G. T. Forcherio, P. Blake, M. Seeram, D. DeJarnette, and D. K. Roper, "Coupled dipole plasmonics of nanoantennas in discontinuous, complex dielectric environments," *Journal of Quantitative Spectroscopy and Radiative Transfer*, vol. 166, pp. 93–101, 2015.

[58] D. DeJarnette, D. K. Roper, and B. Harbin, "Geometric effects on far-field coupling between multipoles of nanoparticles in square arrays," *Journal of the Optical Society of America B*, vol. 29, no. 1, pp. 88–100, 2012.

[59] D. Dejarnette, G. G. Jang, P. Blake, and D. K. Roper, "Polarization angle affects energy of plasmonic features in Fano resonant regular lattices," *Journal of Optics*, vol. 16, no. 10, Article ID 105006, 2014.

[60] P. Blake, J. Obermann, B. Harbin, and D. K. Roper, "Enhanced nanoparticle response from coupled dipole excitation for plasmon sensors," *IEEE Sensors Journal*, vol. 11, no. 12, pp. 3332–3340, 2011.

[61] H. Ebadi-Dehaghani and M. Nazempour, "Thermal conductivity of nanoparticles filled polymers," in *Smart Nanoparticles Technology*, A. Hashim, Ed., chapter 23, pp. 519–534, INTECH, Rijeka, Croatia, 2012.

[62] J. E. Mark, *Polymer Data Handbook*, vol. 131, no. 44, Oxford University Press, New York, NY, USA, 2nd edition, 2009.

[63] K. Buschow, "Gold properties," in *Encyclopedia of Materials—Science and Technology*, p. 3595, Elsevier, New York, NY, USA, 2001.

[64] L. A. Girifalco, *Statistical Mechanics of Solids*, Oxford University Press Inc, New York, NY, USA, 2000.

[65] M. Born and E. W. Wolf, *Principles of Optics*, Cambridge University Press, Cambridge, UK, 1999.

[66] P. J. Coelho, "The role of ray effects and false scattering on the accuracy of the standard and modified discrete ordinates methods," *Journal of Quantitative Spectroscopy and Radiative Transfer*, vol. 73, no. 2-5, pp. 231–238, 2002.

[67] A. Ishimaru, *Wave Propagation and Scattering in Random Media*, vol. 8, no. 4, John Wiley & Sons, New York, NY, USA, 1978.

[68] J. C. Norman, D. F. Dejarnette, and D. K. Roper, "Polylogarithm-based computation of Fano resonance in arrayed dipole scatterers," *The Journal of Physical Chemistry C*, vol. 118, no. 1, pp. 627–634, 2014.

[69] D. DeJarnette, J. Norman, and D. K. Roper, "Attribution of Fano resonant features to plasmonic particle size, lattice constant, and dielectric wavenumber in square nanoparticle lattices," *Photonics Research*, vol. 2, no. 1, pp. 15–23, 2014.

[70] G. A. Niklasson, C. G. Granqvist, and O. Hunderi, "Effective medium models for the optical properties of inhomogeneous materials," *Applied Optics*, vol. 20, no. 1, pp. 26–30, 1981.

[71] O. Levy and D. Stroud, "Maxwell Garnett theory for mixtures of anisotropic inclusions: application to conducting polymers," *Physical Review B*, vol. 56, no. 13, pp. 8035–8046, 1997.

[72] M. A. Kats, R. Blanchard, S. Ramanathan, and F. Capasso, "Thin-film interference in lossy, ultra-thin layers," *Optics and Photonics News*, vol. 25, no. 1, pp. 40–47, 2014.

[73] M. I. Tribelsky, S. Flach, A. E. Miroshnichenko, A. V. Gorbach, and Y. S. Kivshar, "Light scattering by a finite obstacle and fano resonances," *Physical Review Letters*, vol. 100, no. 4, pp. 1–4, 2008.

[74] B. J. Berne and R. Pecora, *Dynamic Light Scattering: With Applications to Chemistry, Biology, and Physics*, Courier Corporation, 2003.

[75] P. H. Oosthuizen and A. Y. Kalendar, *Natural Convective Heat Transfer from Narrow Plates*, SpringerBriefs in Applied Sciences and Technology, Springer, New York, NY, USA, 2013.